World Electric Vehicle Journal

MDPI

Article

Online Estimation of Internal Short Circuit Resistance for Large-Format Lithium-Ion Batteries Combining a Reconstruction Method of Model-Predicted Voltage

Anci Chen, Weige Zhang *, Bingxiang Sun, Hao Li and Xinyuan Fan

National Active Distribution Network Technology Research Center (NANTEC), Beijing Jiaotong University, Beijing 100044, China

* Correspondence: wgzhang@bjtu.edu.cn

Abstract: The resistance of the internal short-circuit (ISC) has a potential evolution trend accompanied by an increasing safety risk. Thus, an accurate online resistance estimation for the ISC is crucial for evaluating its safety risk and taking staged handling measures. Since the ISC battery mainly presents abnormal stage of charge (SOC) depletion behaviors, the SOC estimation processes based on state observers and battery models will act an important basis of the ISC resistance estimation problem. However, as it will be exhibited in this paper, when directly using the measured voltage of the ISC battery as the output variable of the state observer, the battery model error will limit the SOC estimation accuracy and further lead to very inaccurate or even divergent ISC resistance estimation results for large-format batteries, which present quite slight SOC depletion behaviors at the ISC state. To this end, this paper proposes a novel SOC and ISC resistance co-estimation method which combines a reconstruction method of the model-predicted voltage of the ISC battery. Experimental validations are carried out with a 37 Ah battery, results show that the proposed method which uses the reconstructed model-predicted voltage (RMPV) as the output variable of the state observer only present maximum estimation errors of 39.96 Ω and 2.00 Ω for the ISC resistances of 100 Ω and 10 Ω, respectively.

Keywords: lithium-ion battery; internal short-circuit; state estimation

Citation: Chen, A.; Zhang, W.; Sun, B.; Li, H.; Fan, X. Online Estimation of Internal Short Circuit Resistance for Large-Format Lithium-Ion Batteries Combining a Reconstruction Method of Model-Predicted Voltage. *World Electr. Veh. J.* **2022**, *13*, 170. https://doi.org/10.3390/wevj13090170

Academic Editor: Peter Van den Bossche

Received: 28 August 2022
Accepted: 11 September 2022
Published: 13 September 2022

1. Introduction

Lithium-ion batteries have been widely used in electric vehicles (EVs) thanks to their excellent performance on energy density and cycling life [1,2]. However, battery thermal-runaway (TR) accidents have occurred frequently in recent years and thus severely restrict the further popularization of EVs [3–5]. The ISC has been proved one of the major causes of battery TR; consequently, an enormous number of ISC detection methods have been developed to guarantee battery operation safety [6,7]. Moreover, it has been revealed that the ISC presents a potential resistance evolution trend from large to small accompanied by an increasing safety risk [8,9]. Thus, accurately tracking the resistance evolution process after the ISC is detected will be crucial for maximizing the economy of the safe operation of batteries, avoiding any unnecessary introduction of costly intervention measures.

To the best of the authors' knowledge, research on the ISC resistance estimation methods is still in its infancy, only limited literature have been published up to now. Most of the existing methods boil down to the SOC and ISC resistance co-estimation process based on battery models and state observers. Seo et al. [10] utilized the equivalent circuit model (ECM) and Extended Kalman filter (EKF) to realize the online identification of battery open circuit voltage (OCV), so as to obtain the state of charge (SOC) of the ISC battery according to the OCV–SOC mapping relationship and thus the ISC resistance. This method was proved accurate for ISC resistances below 30 Ω. Zheng et al. [11] established a mean-difference model (MDM) for battery packs based on the ECM, then quantitatively

evaluated SOC inconsistency within a battery pack that was based the MDM and EKF, and on this basis a ISC resistance of 13 Ω was accurately estimated. Hu et al. [12] proposed a multi-state fusion ISC resistance estimation method, where the ISC current was firstly estimated through the ECM and EKF based SOC estimation process, then the ISC resistance was estimated by the regression of a ISC current-resistance model. Verification results with a 18,650 battery showed this method could achieve a satisfying accuracy for ISC resistances up to 100 Ω. Moreover, several ISC resistance estimation methods based on special technologies have also been reported, typically including the incremental capacity (IC) curve based method proposed by Qiao et al. [13], as well as the method based on the transformation of voltage curves during charging proposed by Kong et al. [14]. However, these special operation condition-dependent methods can hardly be applied to the online estimation processes.

With regard to the above existing ISC resistance estimation methods, the special technologies based ones as reported in [13,14] rely on the special battery operation conditions; by contrast, the battery models and state observer-based methods will be more applicable to the online estimation processes. However, it should be noted that for the existing battery models and state observer-based methods as introduced above, only ISC resistances below 30 Ω can be accurately estimated in [10,11]; moreover, although the ISC resistance of 100 Ω is accurately estimated in [12], the tested 18650 battery has a fairly small capacity. This is because of the fact that battery models and state observer-based methods achieve the ISC resistance estimation essentially through the joint estimation of battery SOC, so that the ISC-caused abnormal SOC depletion can be quantitatively assessed and thus the ISC resistance can be obtained. In this case, since the SOC estimation accuracy will be limited by the inherent error of battery models, the existing methods can only work for the applications where batteries are with small capacities or the ISC resistances are low. When it comes to the ISC resistance estimation problem for the large-format batteries, the SOC depletion behavior of the ISC will be quite slight, especially when the ISC resistance is high; consequently, it will be buried in the SOC estimation errors causing the failure of the existing methods.

Given the fact that the model error, which restricts the effectiveness of the SOC and ISC resistance co-estimation for large-format batteries with high ISC resistances, lies in the deviation between the model predicted battery voltage and the measured battery voltage, this paper proposed a novel online ISC resistance estimation method which combines the conventional SOC estimation methods with a reconstruction method of the model-predicted voltage of the ISC battery. In the proposed method, the RMPV is obtained on the basis of the model error consistency between the normal battery models and the ISC battery models. By using the RMPV as the output variable of the state observers instead of the measured battery voltage, which is adopted in the existing methods, the limitation of the model error on the SOC and ISC resistance co-estimation accuracy will be significantly mitigated, so that the ISC resistance estimation for large-format batteries can be achieved. The remainder of this paper is organized as follows:

Section 2 introduces related works which discuss modeling methods for normal batteries and ISC batteries, as well as foundation of the SOC estimation based ISC resistance estimation problem. Section 3 introduces the adopted SOC estimation method, the proposed reconstruction method of the model-predicted voltage of the ISC battery, and also the overall ISC resistance estimation method. Section 4 introduces the experiment details and analyses corresponding data acquisition results. Section 5 exhibits the validation results of the proposed method. Section 6 provides a conclusion.

2. Related Works

2.1. Modeling of Normal and ISC Batteries

ECMs are capable of accurately depicting battery voltage responses under specific states with outstanding simplicity [15] and thus underlie the ISC resistance estimation methods. The first-order RC model shown in Figure 1a, which is one of the most used

ECMs for normal batteries, consisting of a controlled voltage source U_{oc} to characterize the relationship between OCV and SOC, a resistor in series R_0 to reflect the lumped ohmic resistance of batteries, and a RC parallel network, including R_1 and C_1 to describe the battery polarization characteristics. When applied to the online ISC resistance estimation scenario, the involved parameters in the first-order RC model should be calibrated in the offline environment first. In this paper, parameters are calibrated utilizing the method in [16]. Based on the first-order RC model, the dynamics of a normal battery can be predicted by

$$\begin{cases} U_{t,n}(t) = U_{oc}(t) + I(t)R_0(t) + U_1(t) \\ R_1(t)C_1(t)\frac{dU_1(t)}{dt} = I(t)R_1(t) - U_1(t) \\ \frac{dz_n(t)}{dt} = \frac{I(t)}{Q_{\max}} \end{cases} \tag{1}$$

where t is time, I is load current, U_t is battery voltage, U_1 is voltage of the RC parallel network, z is battery SOC, $Q_{\max}$ is the maximum useful capacity of the battery, and subscript n represents parameters for normal batteries. Note that all the model parameters, including U_{oc}, R_0, R_1, and C_1, are essentially functions of battery SOC.

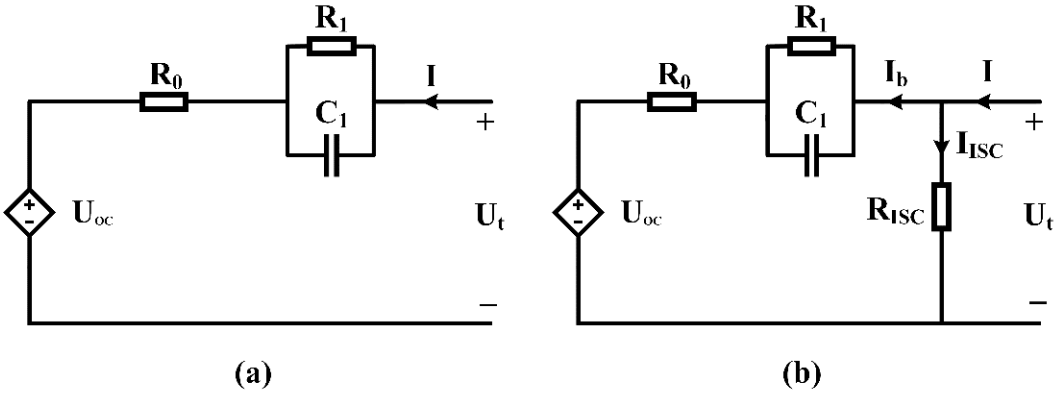

Figure 1. ECMs for: (**a**) Normal batteries; (**b**) ISC batteries.

On the basis of the first-order RC model, the ISC battery is often electrically modeled, as shown in Figure 1b, where a current bypass with a ISC resistor R_{ISC} is added [17,18]. Similarly, the dynamics of the ISC battery can be predicted by

$$\begin{cases} U_{t,f}(t) = \frac{R_{ISC}(t)}{R_0(t)+R_{ISC}(t)}[U_{oc}(t) + I(t)R_0(t) + U_1(t)] \\ R_1(t)C_1(t)\frac{dU_1(t)}{dt} = I(t)R_1(t) - U_1(t) - \frac{R_1(t)}{R_{ISC}(t)}U_{t,f}(t) \\ \frac{dz_f(t)}{dt} = \frac{I(t)}{Q_{\max}} - \frac{U_{t,f}(t)}{R_{ISC}(t)Q_{\max}} \end{cases} \tag{2}$$

where subscript f represents parameters for the ISC batteries.

2.2. Fundamental of Online ISC Resistance Estimation

In order to construct an online ISC resistance estimation problem, according to Equations (1) and (2) in the continuous domain, one can further obtain Equation (3) in the discrete domain.

$$\begin{cases} R_{ISC}(k) = \frac{U_{t,f}(k)}{Q_{\max}\Delta\varepsilon(k)} \\ \Delta\varepsilon(k) = \varepsilon(k) - \varepsilon(k-1) \\ \varepsilon(k) = z_n(k) - z_f(k) \end{cases} \tag{3}$$

where k is sampling instant, ε is SOC depletion state of the ISC (namely the deviation between battery SOC at the normal state and the ISC state), and $\Delta\varepsilon$ is the SOC depletion rate (namely increment of ε in one sampling interval).

Note in Equation (3), z_n, $Q_{\max}$ and $U_{t,f}$ are all observable variables during battery operation, whereas with the charge depletion by an unknown R_{ISC}, z_f cannot be obtained directly. In other words, once z_f can be estimated at every sampling point, the ISC resistance R_{ISC} can be easily calculated using Equation (3). Hence, the ISC resistance estimation can be achieved on basis of the accurate SOC estimation for the ISC battery.

3. Proposed Online ISC Resistance Estimation Method

It should be noted that the model error actually reflects the deviation between the model-predicted battery voltage and the measured battery voltage caused by the model inaccuracy. Meanwhile, the working mechanism of the battery models and state observer-based SOC and ISC resistance co-estimation methods is where the state observer recursively adjusts the SOC estimation result according to the deviation between the model predicted battery voltage and its output variable (the measured battery voltage for conventional methods); therefore, theoretically, this deviation should be caused by the SOC variation relative to the previous time instant. However, when using the measured battery voltage as the system output variable of the state observer, obviously the aforementioned model error will be introduced in this deviation, leading to an inaccurate adjusting of the SOC estimation result. On this basis, it can be inferred that if there is an alternative output variable which is closer to the model-predicted battery voltage compared with the measured battery voltage, the effect of the model error will be mitigated so that the SOC, as well as the ISC resistance estimation performance, can be improved.

To this end, this section will first introduce a conventional particle filter based SOC estimation method. Then a reconstruction method of the model-predicted voltage of the ISC battery will be proposed based on the model error consistency between the normal battery model and the ISC battery model. The RMPV obtained from the proposed reconstruction method will be verified to be much closer to the model-predicted voltage of the ISC battery in Section 5.1. Finally, on the basis of the above two efforts, an online SOC and ISC resistance co-estimation method will be introduced.

3.1. SOC Estimation Method for the ISC Battery

ECMs and state observer-based SOC estimation methods have been widely studied in existing research. In this paper, SOC of the ISC battery is estimated on the basis of the ISC battery model shown in Figure 1b, together with the particle filter (PF), which has been proved a typical state observer, which is superior in SOC estimation accuracy and robustness [19].

With regard to the ISC battery model, in order to implement the SOC estimation, one can make $\mathbf{x}(k) = \begin{bmatrix} U_1(k) & z_f(k) \end{bmatrix}^{\mathrm{T}}$,$\mathbf{u}(k) = \begin{bmatrix} I(k) & U_{t,f}(k) \end{bmatrix}^{\mathrm{T}}$, and $\mathbf{y}(k) = U_{t,f}(k)$, where $\mathbf{x}$, $\mathbf{u}$, and $\mathbf{y}$ denote the state variable matrix, input variable matrix, and output variable matrix, respectively. On this basis, combining the model description given in Equation (2), the discrete state-space function of the ISC battery model can be constructed as

$$\begin{cases} \mathbf{x}_k = \mathbf{A}_{k-1}\mathbf{x}_{k-1} + \mathbf{B}_{k-1}\mathbf{u}_{k-1} \\ \mathbf{y}_k = \mathbf{C}_k\mathbf{x}_k + \mathbf{D}_k\mathbf{u}_k + \mathbf{E}_k \end{cases} \tag{4}$$

where

$$\mathbf{A}_{k-1} = \begin{bmatrix} e^{-\frac{\Delta t}{\tau_{k-1}}} & 0 \\ 0 & 1 \end{bmatrix}, \quad \mathbf{B}_{k-1} = \begin{bmatrix} R_{1,k-1}\left(1 - e^{-\frac{\Delta t}{\tau_{k-1}}}\right) & \frac{R_{1,k-1}}{R_{ISC,k-1}}\left(e^{-\frac{\Delta t}{\tau_{k-1}}} - 1\right) \\ \frac{\Delta t}{Q_{\max}} & -\frac{\Delta t}{R_{ISC,k-1}Q_{\max}} \end{bmatrix}$$

$$\mathbf{C}_k = \begin{bmatrix} \frac{R_{ISC,k}}{R_{0,k}+R_{ISC,k}} & \frac{a_k R_{ISC,k}}{R_{0,k}+R_{ISC,k}} \end{bmatrix}, \quad \mathbf{D}_k = \begin{bmatrix} \frac{R_{0,k}R_{ISC,k}}{R_{0,k}+R_{ISC,k}} \end{bmatrix}, \quad \mathbf{E}_k = \begin{bmatrix} \frac{b_k R_{ISC,k}}{R_{0,k}+R_{ISC,k}} \end{bmatrix}$$

where $\tau = R_1C_1$, Δt is sampling interval, a and b denotes the local linearization coefficients of the OCV-SOC curve making $U_{oc}\left(z_f\right) = az_f + b$, and the time-dependence of variables are described by subscript k for convenience.

With the state-space function in Equation (4), SOC of the ISC battery can be estimated using PF with following procedures:

- Initialization: Set the process noise variance R_w, measurement noise variance R_v, particle population size N; randomly generate N as initial particles $\hat{\mathbf{x}}_0^l$ ($l = 1, 2, \ldots, N$) and set their initial weights $w_k^l = 1/N$.
- Recursively update weights of particles according to Equations (5)–(8).

$$\hat{\mathbf{x}}_k^l = \mathbf{A}_{k-1}^l \hat{\mathbf{x}}_{k-1}^l + \mathbf{B}_{k-1}^l \mathbf{u}_{k-1}^l + \mathbf{w}_{k-1}^l \tag{5}$$

$$\mathbf{e}_k^l = \mathbf{y}_k - \left(\mathbf{C}_k^l \hat{\mathbf{x}}_k^l + \mathbf{D}_k^l \mathbf{u}_k + \mathbf{E}_k^l\right) \tag{6}$$

$$w_k^l = \frac{w_{k-1}^l}{\sqrt{2\pi R_v}} \exp\left(-\frac{\mathbf{e}_k^l \left[\mathbf{e}_k^l\right]^{\mathrm{T}}}{2R_v}\right) \tag{7}$$

$$\overline{w}_k^l = w_k^l / \sum_{l=1}^{N} w_k^l \tag{8}$$

where $\mathbf{w} = \begin{bmatrix} 0 & \mathrm{N}(0, R_w) \end{bmatrix}^{\mathrm{T}}$; $\mathrm{N}(0, R_w)$ is the randomly sampling result from a normal distribution with a zero mean and R_w variance; $\mathbf{e}^l$ represents the system innovation matrix; and $\overline{w}$ represents the normalized weights of particles.

- Resampling of particles: particle degradation is a common phenomenon of the PF, resulting in a decrease in the number of effective particles. It can be evaluated according to the following indicator:

$$w_k^{eff} = 1 / \sum_{l=1}^{N} \left(\overline{w}_k^l\right)^2 \tag{9}$$

Once the indicator w_k^{eff} is lower than the given threshold wth at a certain instant k, the particles need a resampling process to keep their effectiveness. The System Resampling Method is adopted in this paper, referring to [20], and weights of particles after resampling need to be re-assigned according to

$$\overline{w}_k^l = 1/N \tag{10}$$

- Recursively update system state estimation result: update the system state estimation result according to the Monte Carlo integration, written as

$$\hat{\mathbf{x}}_k = \sum_{l=1}^{N} \overline{w}_k^l \hat{\mathbf{x}}_k^l \tag{11}$$

By extracting $\hat{z}_{f,k}$ from the estimated system state variable matrix $\hat{\mathbf{x}}_k$ at each iteration, the SOC of the ISC battery can be obtained.

3.2. Reconstruction Method of the Model-Predicted Voltage of the ISC Battery

ISC resistance estimation relies on an accurate SOC estimation for the ISC battery. However, the inherent deviation between the model predicted and the measured voltage of the ISC battery (i.e., model inaccuracy) will induce a significant error into the SOC estimation process through Equation (6). From another point of view, if it is possible to use the model-predicted voltage $\hat{U}_{t,f}$ instead of the measured voltage $U_{t,f}$ as the system output,

the effect of the model inaccuracy will be eliminated and the SOC estimation accuracy will be 100% in theory.

Whereas the ISC battery model cannot be used to predict the voltage responses of the ISC battery practically since R_{ISC} is the variable needing to be estimated, the lack of the ISC depiction capability of the normal battery model will cause a distortion in its predicted voltage. However, note that the normal battery model and the ISC battery model has an identical kernel and their only difference lies in the introduction of R_{ISC}. This reveals the fact that if R_{ISC} is known, the ISC battery model and the normal battery model should have quite consistent model error characteristics when applied to depict the voltage responses of the ISC battery and the normal battery, respectively. On this basis, we propose a reconstruction method of the model-predicted voltage for the ISC battery to help improve the SOC and thus the ISC resistance estimation accuracy, described as follows.

For a battery pack consisting of n batteries in series where battery j is the ISC battery, use the normal battery model to predict voltage responses of all the normal batteries. Supposing R_{ISC} is known and the model-predicted voltage $\hat{U}_t^j$ of cell j is obtained from the ISC battery model (where both R_{ISC} and $\hat{U}_t^j$ are unknown), then based on the above analysis of model error consistency, we can further make an assumption that model error of the ISC battery equals the mean value of model errors of all the batteries, namely

$$E_t^j(k) = \sum_{i=1}^{n} E_t^i(k)/n \tag{12}$$

where the model error of each battery is defined by $E_t^i = \hat{U}_t^i - U_t^i$.

Note that the measured voltages U_t^i of each battery and model predicted voltages $\hat{U}_t^i (i \neq j)$ of normal batteries are accessible during battery operation, thus the model-predicted voltage of the ISC battery can be reconstructed by the further transformation of Equation (12), yielding

$$\hat{U}_{t,rct}^j(k) = U_t^j(k) + \sum_{i=1,i\neq j}^{n} E_t^i(k)/(n-1) \tag{13}$$

where $\hat{U}_{t,rct}^j$ is the reconstruction result of the model-predicted voltage, namely the RMPV.

3.3. Online SOC and ISC Resistance Co-estimation Method

Based on the above analysis, an online ISC resistance estimation method is proposed with its overall scheme is shown in Figure 2. Its workflow can be described as follows:

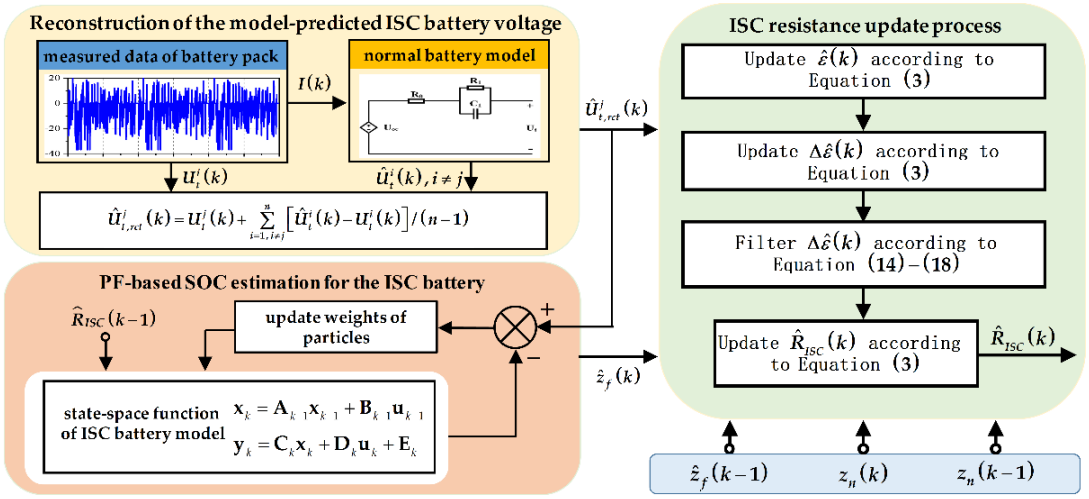

Figure 2. Overall scheme of the proposed online ISC resistance estimation method.

- Initialization: Set the value of $\hat{R}_{ISC}(0)$ and initialize PF, as introduced in Section 3.1.
- Recursively update the operation data of the battery pack, including the measured load current $I(k)$ and voltage of each battery $U_t^i(k)$. Meanwhile, input $I(k)$ into the normal battery model to obtain the model-predicted voltage of normal batteries $\hat{U}_t^i(k)(i \neq j)$.
- Update the RMPV of the ISC battery $\hat{U}_{t,rct}^j(k)$ according to Equation (13).
- Update $\hat{z}_f(k)$ through the PF-based SOC estimation process for the ISC battery as introduced in Section 3.1. Importantly, in this step, the measured voltage of the ISC battery $U_t^j(k)$ is replaced with the RMPV $\hat{U}_{t,rct}^j(k)$ as the system output variable, namely making $\mathbf{y}(k) = \hat{U}_{t,rct}^j(k)$.
- Update $\hat{\varepsilon}(k)$ and $\Delta\hat{\varepsilon}(k)$ in turn according to Equation (3), respectively.
- Although noises will be eliminated by the PF to a great certain, the residual noises induced in $\Delta\hat{\varepsilon}(k)$ whose calculation process contains a backward differential for $\hat{z}_f(k)$ will become significant relative to the slight true value. Thus, $\Delta\hat{\varepsilon}(k)$ needs to be further filtered to obtain the final ISC resistance estimation result. The Kalman filter (KF) is adopted in this paper, which has an excellent filtering ability for white noise [21]. The KF based filtering process for $\Delta\hat{\varepsilon}(k)$ can be achieved according to Equations (14)–(18).

$$\widetilde{\Delta\hat{\varepsilon}}(k^-) = \widetilde{\Delta\hat{\varepsilon}}(k-1) + \Delta\hat{\varepsilon}(k) \tag{14}$$

$$P(k^-) = P(k-1) + Q \tag{15}$$

$$K(k) = P(k^-)\left[P(k^-) + R\right]^{-1} \tag{16}$$

$$\widetilde{\Delta\hat{\varepsilon}}(k) = \widetilde{\Delta\hat{\varepsilon}}(k^-) + K(k)\left[\Delta\varepsilon(k) - \widetilde{\Delta\hat{\varepsilon}}(k^-)\right] \tag{17}$$

$$P(k) = P(k^-) - K(k)P(k^-) \tag{18}$$

where $\widetilde{\Delta\hat{\varepsilon}}$ is the filtered result of $\Delta\hat{\varepsilon}$, P is the state variance of the filter, and Q and R denote the variances of the process noises and measurement noises, respectively.

- Update the ISC resistance estimation result $\hat{R}_{ISC}(k)$ by substituting $\widetilde{\Delta\hat{\varepsilon}}(k)$ and $\hat{U}_{t,rct}^j(k)$ into Equation (3).

4. Data Acquisition

4.1. Experiment Details

Experiments are implemented with a battery module consisting of seven NMC batteries with rated capacity of 37 Ah. The tested battery module is enclosed in a SPX-150BIII thermal chamber to acquire the desired test temperature of 25 °C. The current profile shown in Figure 3, which comprehensively covers the typical battery operating conditions including FUDS cycles, rest stages, and multi-step charging stages, is applied to the battery module via a Arbin BT2000 battery tester. The voltage of each battery and load current of the battery module during test are also sampled by the tester with errors of less than 0.1%. The commonly used equivalent resistor (ER) approach is adopted to implement the equivalent ISC tests [22–24], where an equivalent short circuit resistor and a switch and are connected externally with battery 4 to simulate its ISC behavior, as shown in Figure 4. It has been pointed out that the ISC resistance lies in the 100 Ω magnitude at the early ISC stage, and battery safety risk is significant when it falls below 10 Ω [25,26]. This indicates that it is crucial for estimation methods to have the capability of accurately estimating ISC resistances between 100 Ω~10 Ω. Thus, a 100 Ω-ER and a 10 Ω-ER are adopted in this paper to verify the performance of the proposed estimation method.

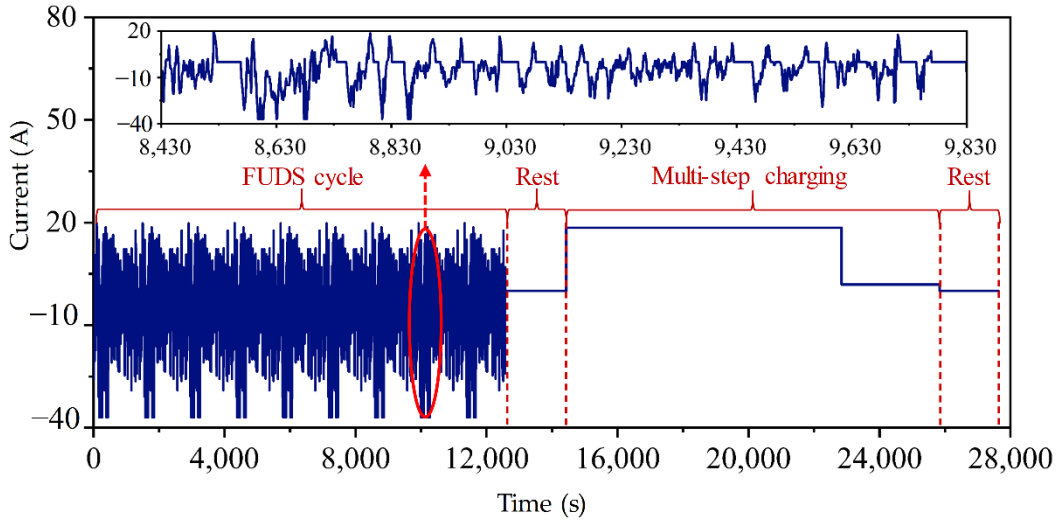

Figure 3. Current profile used for test.

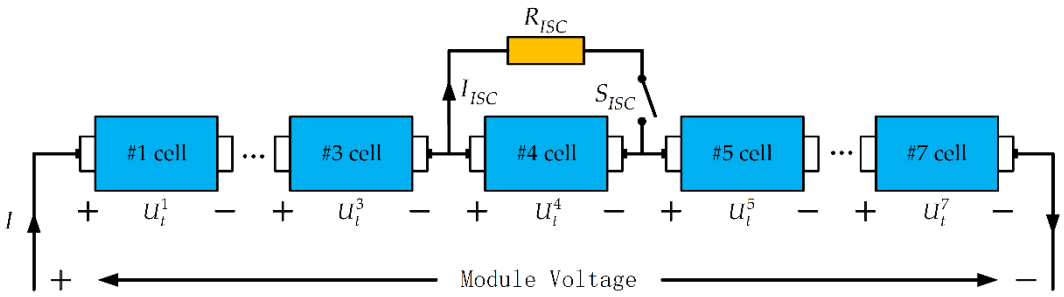

Figure 4. Scheme of the ER approach for the equivalent ISC test.

4.2. Results Discussion

Figure 5 exhibits the voltage data of the tested battery module acquired from the 100 Ω-ER test and the 10 Ω-ER test, where those solid lines are voltage curves measured by the tester and those dotted lines are voltage curves predicted by the normal battery model. As can be seen in Figure 5a, the measured voltage curves and normal battery model predicted voltage curves coincide well. In particular, abnormalities in the measured voltage curve of battery 4 can hardly be observed, since the ISC current is slight with a 100 Ω-ER, so that only a very limited SOC depletion and consequent voltage abnormality is caused during the whole test process. The results of the 10 Ω-ER test is more intuitive, as exhibited in Figure 5b. The measured voltage curve of battery 4 gradually decreases out of the group as the test goes on, whereas the voltage curves of the other batteries in the module as well as the normal model predicted voltage curve of battery 4 still show a high consistency during the test process. Data involved in Figure 5 were used for the validation of the proposed ISC resistance estimation method.

Figure 6 further exhibits the model error distributions of each battery according to the measured and normal model predicted voltage data in Figure 5. Apart from battery 4, the model errors of the other batteries during both the 100 Ω-ER test and the 10 Ω-ER test distribute in the range of −0.017 V~0.011 V with a significant consistence, whereas the model errors of battery 4 gradually deviate from the group as the test goes on, since the normal battery model lacks the ability to depict the ISC behavior. Figure 6 exhibits the distortion phenomenon of the predicted voltage of the normal battery model when the ISC occurs; this is the reason why a reconstruction method is needed to help improve the SOC and ISC resistance estimation accuracy. Additionally, the significant consistency among the model errors of normal batteries helps the understanding of the rationality of the proposed reconstruction method.

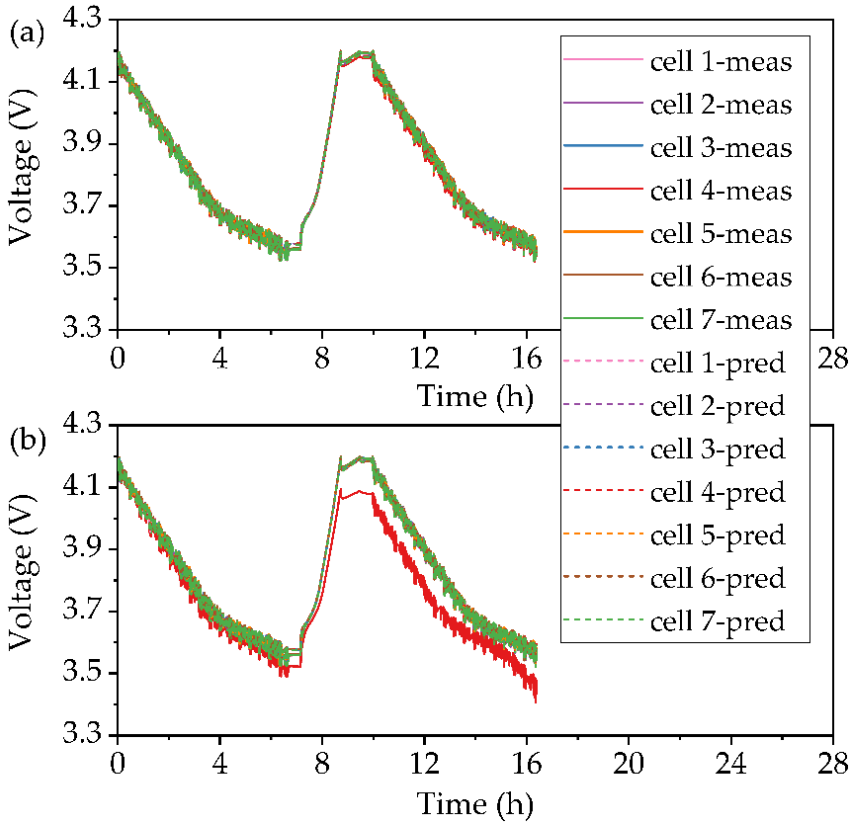

Figure 5. Voltage responses of each battery during: (**a**) 100 Ω-ER ISC test; (**b**) 10 Ω-ER ISC test.

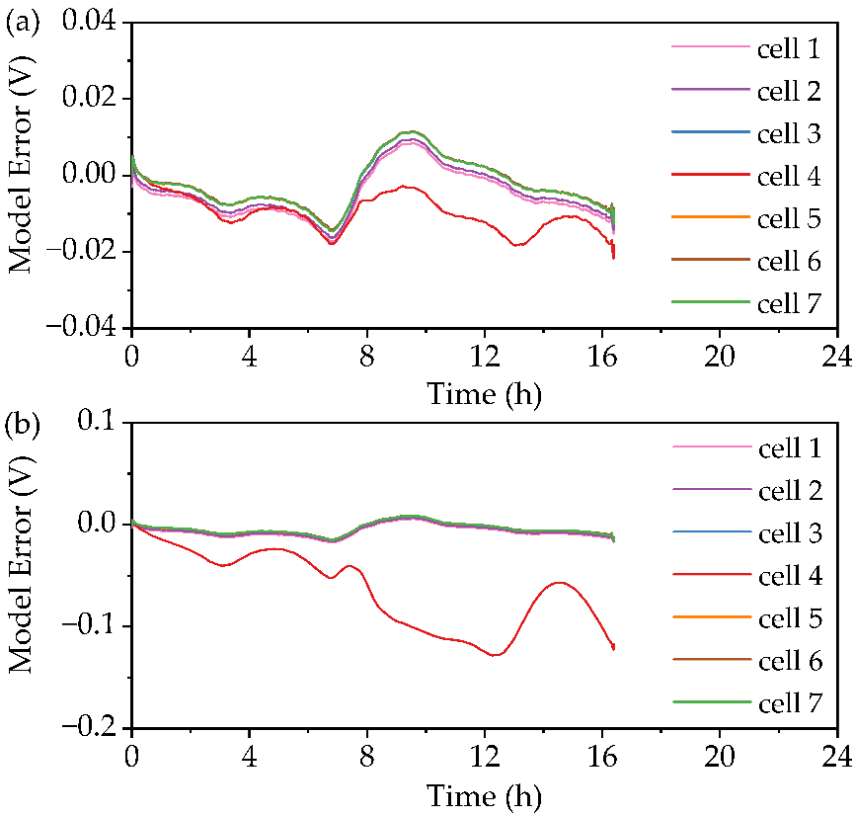

Figure 6. Model errors of each battery during: (**a**) 100 Ω-ER ISC test; (**b**) 10 Ω-ER ISC test.

5. Method Validation

In this section, the measured voltage is referred to as MV for convenience.

5.1. Validation of RMPV

Figure 7 demonstrates the performance of the proposed reconstruction method of the model-predicted voltage of the ISC battery. Note that the resistances of the adopted ERs are known, thus the reference values in Figure 7 are obtained from the ISC battery model with given ISC resistances. Figure 7a,c exhibits the reconstruction results during the 100 Ω-ER test and 10 Ω-ER test, respectively. Since battery voltage varies within a wide range, it is hard to visualize the reconstruction performance. Therefore, Figure 7b,d further exhibits the voltage errors of the RMPV and MV relative to the reference values during the 100 Ω-ER test and 10 Ω-ER test, respectively. During the 100 Ω-ER test, the MV presents voltage errors range from −0.014 V to 0.007 V, by comparison, the RMPV only presents voltage errors within the range of −0.003 V~0 V, whereas during the 10 Ω-ER test, the voltage errors of the MV lies in the range of −0.014 V~0.006 V, while that of the RMPV are distributed in the range of −0.006 V~0.002 V. The consistent voltage errors of the MV of the ISC battery during 100 Ω-ER test and 10 Ω-ER test along with the model errors of normal batteries, as introduced in Section 4.2, support the above statement that when the ISC resistance is given, the ISC battery model and the normal battery model should have quite consistent model error characteristics. Moreover, reconstruction results exhibited in Figure 7 demonstrate that the RMPV is much closer to that predicted by the ISC battery model compared with the MV; this will help to improve the SOC and ISC resistance estimation accuracy when using the RMPV as the output variable of the state observer.

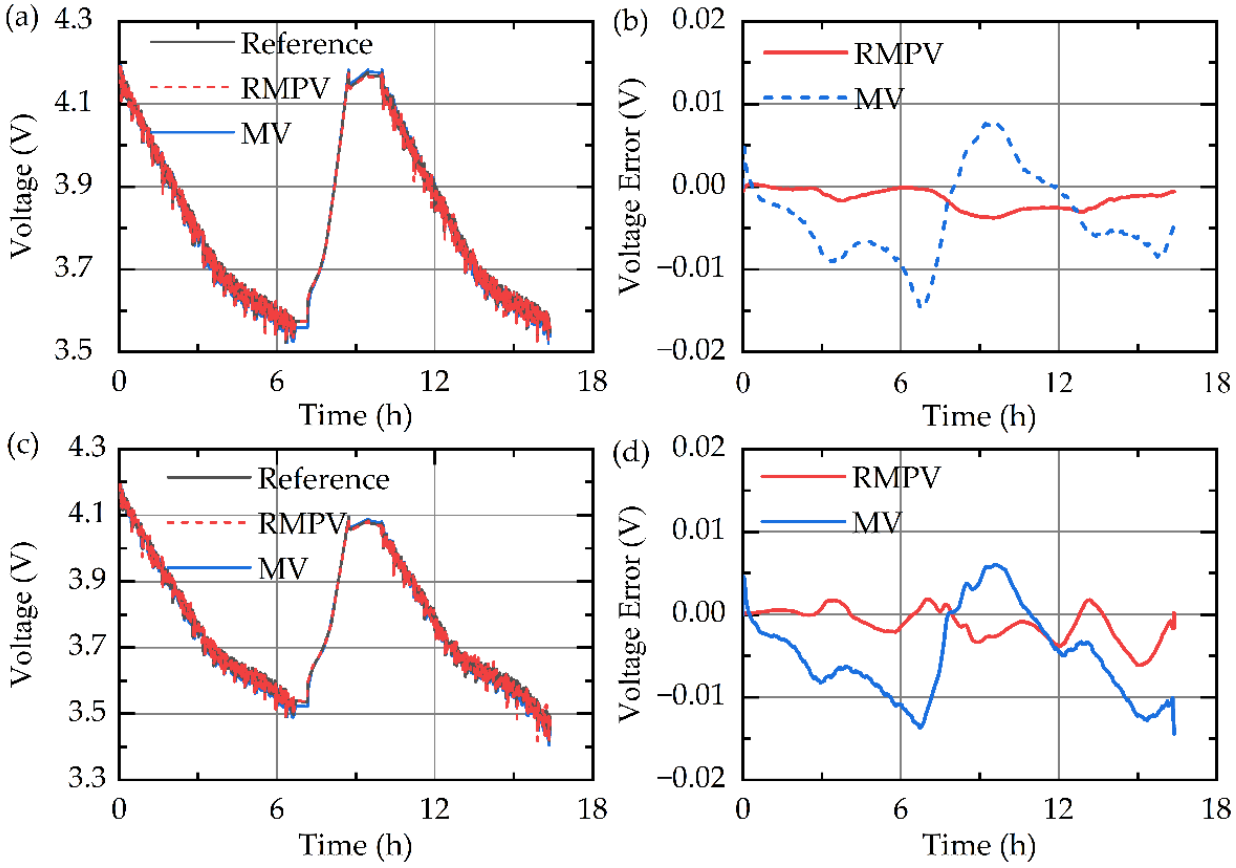

Figure 7. Performance of the proposed reconstruction method for the model-predicted voltage of the ISC battery: (**a**) reconstruction result during the 100 Ω-ER test; (**b**) voltage error relative to the reference value during the 100 Ω-ER test; (**c**) reconstruction result during the 10 Ω-ER test; (**d**) voltage error relative to the reference value during the 10 Ω-ER test.

5.2. Validation of SOC and ISC resistance Estimation Accuracy

Figure 8 exhibits the overall estimation results during the 100 Ω-ER test. As can be seen in Figure 8a, the SOC estimation results of the ISC battery with both the proposed RMPV-based method and the conventional MV-based method converge around the true value, whereas that of the RMPV-based method shows a better consistency with the true value. Figure 8b exhibits the estimation results of ε based on the SOC estimation results; here it can be seen that estimation result of ε with the RMPV-based method achieves a much higher accuracy, whereas that with the MV-based method deviates remarkably from the reference curve. Note that the estimation inaccuracy of the MV-based method is actually only within 0.03%, only the true value is much more slight. Figure 8c further exhibits the estimation results of Δε, where significant noises can be seen both with the RMPV-based method and the MV-based method. The cause of this phenomenon has been stated in Section 3.3. Moreover, although the filtering results of two methods overlap to a great degree visually due to the axis range, it can still be observed that the RMPV-based result has a higher consistency with the true value. Figure 8d gives the final ISC resistance estimation results, where the RMPV-based method presents estimation results from 60 Ω to 129 Ω; however, the MV-based method presents a much more inaccurate result and diverges in the time quantum of 8 h~12 h, during which the inaccurate estimation result of ε presents a downward trend.

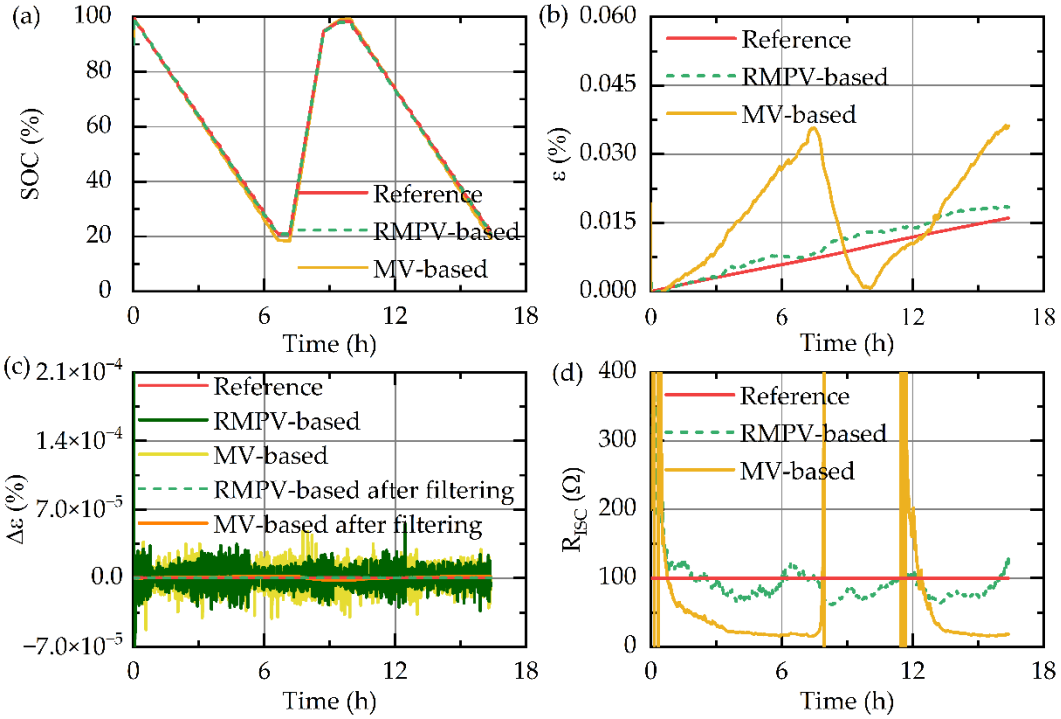

Figure 8. Estimation results during the 100 Ω-ER test: (**a**) SOC estimation result; (**b**) estimation result of ε; (**c**) estimation result of Δε; (**d**) R_{ISC} estimation result.

Further, Figure 9 exhibits the overall estimation results during the 10 Ω-ER test. The estimation results of SOC and Δε are visually similar to those seen in the 100 Ω-ER test; thus, corresponding descriptions will not be repeated here. However, as shown in Figure 9b, the MV-based estimation result of ε presents higher consistency with the true value compared with that of the 100 Ω-ER test. Note that the absolute inaccuracy of the MV-based method does not decrease; the true value simply increases under 10 Ω-ER, causing the error ratio to become smaller. Figure 9d exhibits the ISC resistance estimation results during the 10 Ω-ER test, where the RMPV-based result is distributed in the range of 8 Ω~11 Ω, and although the MV-based result does not go into divergence, it lies within a much wider range of 6 Ω~92 Ω.

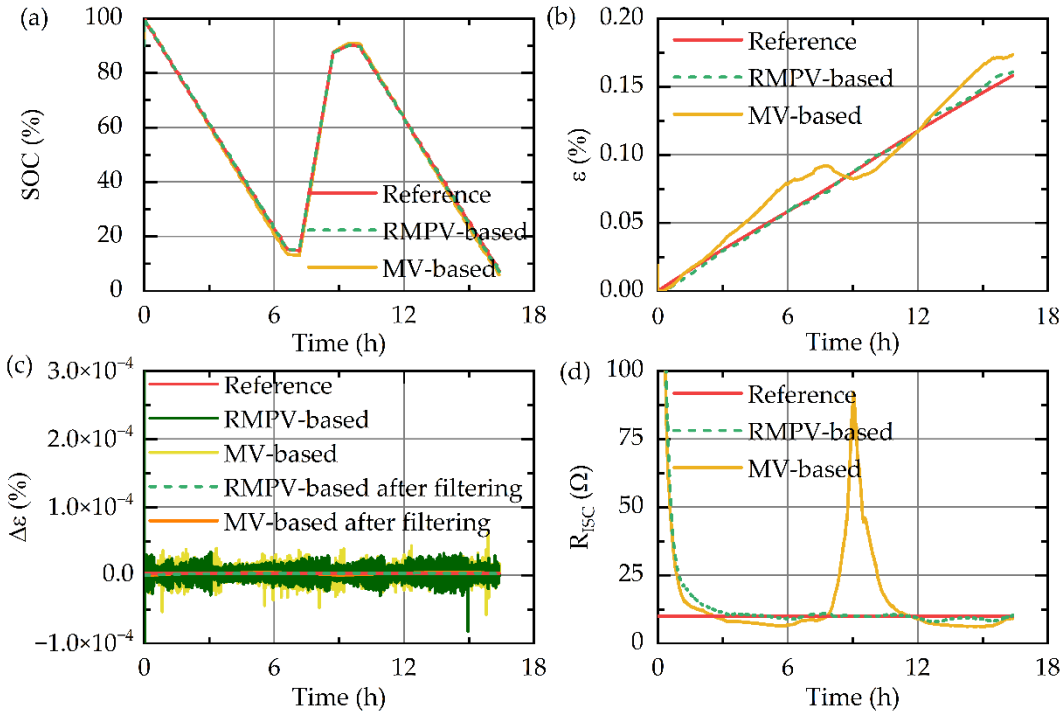

Figure 9. Estimation results with a 10 Ω-ER: (**a**) SOC estimation result; (**b**) estimation result of ε; (**c**) estimation result of Δε; (**d**) R_{ISC} estimation result.

Finally, as the key process of the ISC resistance estimation, the SOC estimation performances of the two methods during the 100 Ω-ER test and the 10 Ω-ER test are listed in Table 1 in terms of mean absolute error (MAE) and maximum absolute error (MAAE), respectively. Similarly, Table 2 lists MAE and MAAE of the final ISC resistance estimation result of two methods. Note that considering the MV-based ISC resistance result diverges in a part of time during the 100 Ω-ER test, corresponding data are thus not considered in the statistic processes.

Table 1. Statics of SOC estimation errors.

Statistics	100 Ω-ER Test		10 Ω-ER Test	
	RMPV-Based	MV-Based	RMPV-Based	MV-Based
MAE (%)	0.20	1.01	0.21	1.00
MAAE (%)	0.37	2.86	0.69	2.12

Table 2. Statics of ISC resistance estimation errors.

Statistics	100 Ω-ER Test		10 Ω-ER Test	
	RMPV-Based	MV-Based	RMPV-Based	MV-Based
MAE (Ω)	18.47	80.94	0.65	7.74
MAAE (Ω)	39.96	84.92	2.00	82.28

5.3. Validation of Tracking Capability to ISC Resistance Variation

Apart from the estimation accuracy with regard to a constant ISC resistance, the tracking capability in regard to ISC resistance variation is also a key indicator for an estimation method. Figure 10 exhibits the tracking capability of the proposed RMPV-based estimation method during a sudden-changing ER test where a 100 Ω-ER test is implemented first and the ER is changed to 10 Ω about 9.5 h later. As it can be seen in Figure 10a,b, the estimation results of the SOC and ε follow their true values well during the test. However,

in Figure 10c, the filtered estimation result of $\Delta\varepsilon$ does not response immediately when its true value suddenly changes along with the changing of ER. This is because the existence of KF, which is adopted to eliminate the noises included in the estimation result of $\Delta\varepsilon$, makes the estimation method insensitive to the sudden change of $\Delta\varepsilon$ at the same time. Consequently, as shown in Figure 10d, the proposed method presents an adjustment time of about 2.5 h. It should be noted that the situation discussed above is an extreme one, whereas the evolution of the ISC resistance will occur as a gradual process and can last for hundreds of hours in practice [27], thus it can be inferred that the adjustment time of the proposed method will not cause any limitation on its effectiveness. Moreover, in terms of the tracking capability which has been pointed out to be only decided through the filtering process of $\Delta\varepsilon$, the conventional MV-based method will have the same performance as the proposed RMPV-based method and therefore is not discussed here.

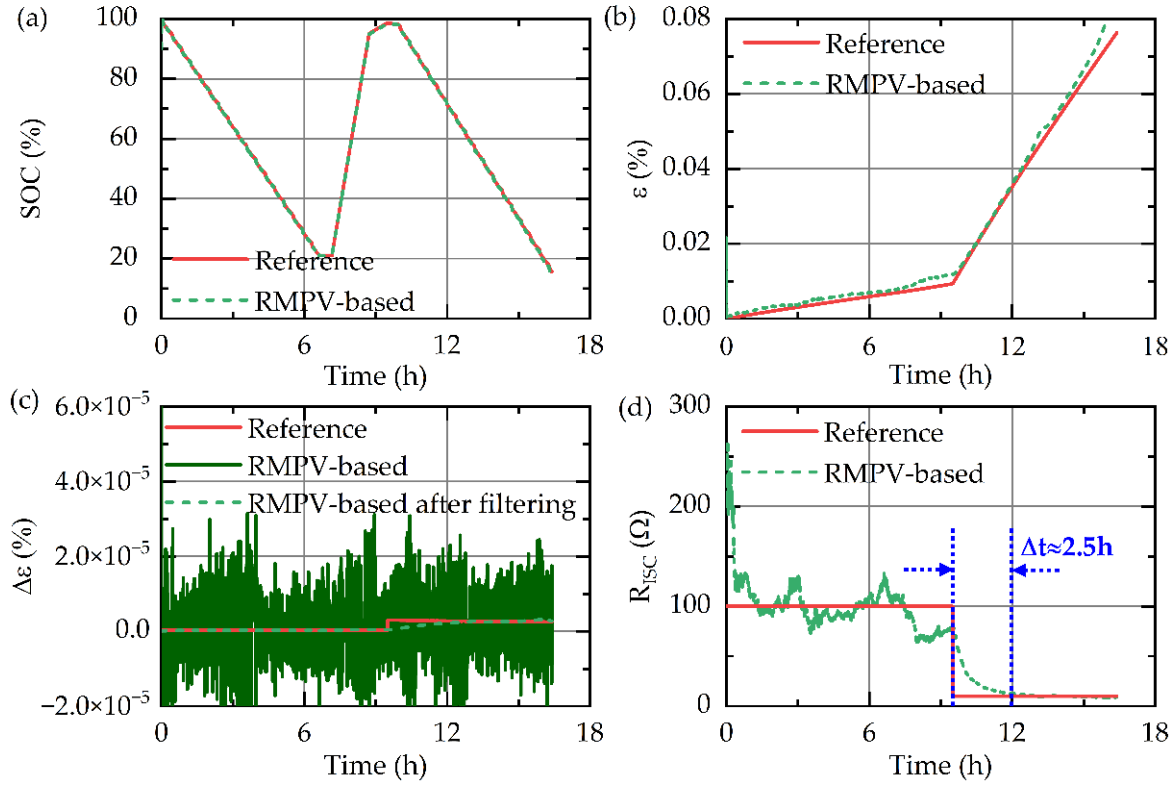

Figure 10. Estimation results with a sudden-changing ER from 100 Ω to 10 Ω: (**a**) SOC estimation result; (**b**) calculation result of ε; (**c**) calculation result of $\Delta\varepsilon$; (**d**) R_{ISC} estimation result.

6. Conclusions

This paper proposed a RMPV-based online ISC resistance estimation method for large-format lithium-ion batteries. A PF-based SOC estimation method for the ISC battery is first introduced as the basis of the proposed method. However, it is well known that the SOC estimation is limited by the inherent model inaccuracy, since the state observer (PF in this paper) is with a kernel of the state-space function of the ISC battery model. This will cause the slight SOC depletion behavior of a large-format ISC battery to be buried in the SOC estimation error and thus lead to a failure of the ISC resistance estimation.

With regard to this difficulty, a model error consistency based reconstruction method is proposed, which utilizes the normal model predicted voltage of the normal batteries inside the battery pack along with the MV of all the batteries to reconstruct the model-predicted voltage of the ISC battery, which is supposed to be given by the ISC battery model when the ISC resistance is known. On this basis, the above model inaccuracy effect can be significantly mitigated by using the RMPV as the output variable of the state observer instead of the MV.

Experimental validation results show that the proposed RMPV-based method can achieve a significant improvement of the ISC resistance estimation accuracy compared with the conventional MV-based method. Specifically, the MAE and MAAE of the proposed method are 18.47 Ω and 39.96 Ω, respectively, with regard to a ISC resistance of 100 Ω. By comparison, the conventional method goes diverges during part of the estimation process, where the estimated SOC depletion state of the ISC battery presents a downward trend caused by the SOC estimation inaccuracy. Consequently, the MAE and MAAE of the estimation result of the conventional method increase to 80.94 Ω and 84.92 Ω, respectively (data in the divergent area not concluded). With regard to a ISC resistance of 10 Ω, the proposed method achieves an MAE and MAAE of 0.65 Ω and 2 Ω, respectively, whereas those of the conventional method are 7.74 Ω and 82.28 Ω, respectively. The tracking capability of the proposed method to the ISC resistance variation is also experimentally validated, and results show when the ISC resistance suddenly changes from 100 Ω to 10 Ω, the proposed method only presents an adjustment time of about 2.5 h. This is insignificant relative to the gradual evolution process, which can last for hundreds of hours in practice. In conclusion, the proposed method will provide an effective option for the ISC resistance estimation problem in large-format battery applications.

Author Contributions: Conceptualization, W.Z.; methodology, A.C.; investigation, A.C.; writing—original draft preparation, A.C.; writing—review and editing, B.S.; visualization, H.L. and X.F. All authors have read and agreed to the published version of the manuscript.

Funding: This research was funded by National Natural Science Foundation of China: 52177206, and National Natural Science Foundation of China: 51907005.

Institutional Review Board Statement: Not applicable.

Informed Consent Statement: Not applicable.

Data Availability Statement: Not applicable.

Conflicts of Interest: The authors declare no conflict of interest. The funders had no role in the design of the study; in the collection, analyses, or interpretation of data; in the writing of the manuscript; or in the decision to publish the results.

References

1. Lu, L.; Han, X.; Li, J.; Hua, J.; Ouyang, M. A Review on the Key Issues for Lithium-Ion Battery Management in Electric Vehicles. *J. Power Sources* **2013**, *226*, 272–288. [CrossRef]
2. Hannan, M.A.; Hoque, M.M.; Mohamed, A.; Ayob, A. Review of Energy Storage Systems for Electric Vehicle Applications: Issues and Challenges. *Renew. Sustain. Energy Rev.* **2017**, *69*, 771–789. [CrossRef]
3. Hollmotz, L. Safety of Lithium Ion Batteries in Vehicles–State of the Art, Risks and Trends. In Proceedings of the 23rd International Technical Conference on the Enhanced Safety of Vehicles, Seoul, Korea, 27–30 May 2013.
4. Wang, Q.; Ping, P.; Zhao, X.; Chu, G.; Sun, J.; Chen, C. Thermal Runaway Caused Fire and Explosion of Lithium Ion Battery. *J. Power Sources* **2012**, *208*, 210–224. [CrossRef]
5. Feng, X.; Ouyang, M.; Liu, X.; Lu, L.; Xia, Y.; He, X. Thermal Runaway Mechanism of Lithium Ion Battery for Electric Vehicles: A Review. *Energy Storage Mater.* **2018**, *10*, 246–267. [CrossRef]
6. Lai, X.; Jin, C.; Yi, W.; Han, X.; Feng, X.; Zheng, Y.; Ouyang, M. Mechanism, Modeling, Detection, and Prevention of the Internal Short Circuit in Lithium-Ion Batteries: Recent Advances and Perspectives. *Energy Storage Mater.* **2021**, *35*, 470–499. [CrossRef]
7. Zhang, G.; Wei, X.; Tang, X.; Zhu, J.; Chen, S.; Dai, H. Internal Short Circuit Mechanisms, Experimental Approaches and Detection Methods of Lithium-Ion Batteries for Electric Vehicles: A Review. *Renew. Sustain. Energy Rev.* **2021**, *141*, 110790. [CrossRef]
8. Darcy, E. Screening Li-Ion Batteries for Internal Shorts. *J. Power Sources* **2007**, *174*, 575–578. [CrossRef]
9. Liu, L.; Feng, X.; Rahe, C.; Li, W.; Lu, L.; He, X.; Sauer, D.U.; Ouyang, M. Internal Short Circuit Evaluation and Corresponding Failure Mode Analysis for Lithium-Ion Batteries. *J. Energy Chem.* **2021**, *61*, 269–280. [CrossRef]
10. Seo, M.; Goh, T.; Park, M.; Kim, S.W. Detection Method for Soft Internal Short Circuit in Lithium-Ion Battery Pack by Extracting Open Circuit Voltage of Faulted Cell. *Energies* **2018**, *11*, 1669. [CrossRef]
11. Zheng, Y.; Luo, Q.; Cui, Y.; Dai, H.; Han, X.; Feng, X. Fault Identification and Quantitative Diagnosis Method for Series-Connected Lithium-Ion Battery Packs Based on Capacity Estimation. *IEEE Trans. Ind. Electron.* **2022**, *69*, 3059–3067. [CrossRef]
12. Hu, J.; He, H.; Wei, Z.; Li, Y. Disturbance-Immune and Aging-Robust Internal Short Circuit Diagnostic for Lithium-Ion Battery. *IEEE Trans. Ind. Electron.* **2021**, *69*, 1988–1999. [CrossRef]

13. Qiao, D.; Wang, X.; Lai, X.; Zheng, Y.; Wei, X.; Dai, H. Online Quantitative Diagnosis of Internal Short Circuit for Lithium-Ion Batteries Using Incremental Capacity Method. *Energy* **2022**, *243*, 123082. [CrossRef]
14. Kong, X.; Zheng, Y.; Ouyang, M.; Lu, L.; Li, J.; Zhang, Z. Fault Diagnosis and Quantitative Analysis of Micro-Short Circuits for Lithium-Ion Batteries in Battery Packs. *J. Power Sources* **2018**, *395*, 358–368. [CrossRef]
15. Liu, S.; Jiang, J.; Shi, W.; Ma, Z.; Wang, L.Y.; Guo, H. Butler-Volmer-Equation-Based Electrical Model for High-Power Lithium Titanate Batteries Used in Electric Vehicles. *IEEE Trans. Ind. Electron.* **2015**, *62*, 7557–7568. [CrossRef]
16. Chen, A.; Zhang, W.; Zhang, C.; Huang, W.; Liu, S. A Temperature and Current Rate Adaptive Model for High-Power Lithium-Titanate Batteries Used in Electric Vehicles. *IEEE Trans. Ind. Electron.* **2020**, *67*, 9492–9502. [CrossRef]
17. Meng, J.; Boukhnifer, M.; Delpha, C.; Diallo, D. Incipient Short-Circuit Fault Diagnosis of Lithium-Ion Batteries. *J. Energy Storage* **2020**, *31*, 101658. [CrossRef]
18. Ouyang, M.; Zhang, M.; Feng, X.; Lu, L.; Li, J.; He, X.; Zheng, Y. Internal Short Circuit Detection for Battery Pack Using Equivalent Parameter and Consistency Method. *J. Power Sources* **2015**, *294*, 272–283. [CrossRef]
19. Hannan, M.A.; Lipu, M.S.H.; Hussain, A.; Mohamed, A. A Review of Lithium-Ion Battery State of Charge Estimation and Management System in Electric Vehicle Applications: Challenges and Recommendations. *Renew. Sustain. Energy Rev.* **2017**, *78*, 834–854. [CrossRef]
20. Kitagawa, G. Monte Carlo Filter and Smoother for Non-Gaussian Nonlinear State Space Models. *J. Comput. Graph. Stat.* **1996**, *5*, 1–25.
21. Kalman, R.E. A New Approach to Linear Filtering and Prediction Problems. *J. Basic Eng.* **1960**, *82*, 35–45. [CrossRef]
22. Zheng, Y.; Lu, Y.; Gao, W.; Han, X.; Feng, X.; Ouyang, M. Micro-Short-Circuit Cell Fault Identification Method for Lithium-Ion Battery Packs Based on Mutual Information. *IEEE Trans. Ind. Electron.* **2021**, *68*, 4373–4381. [CrossRef]
23. Gao, W.; Zheng, Y.; Ouyang, M.; Li, J.; Lai, X.; Hu, X. Micro-Short-Circuit Diagnosis for Series-Connected Lithium-Ion Battery Packs Using Mean-Difference Model. *IEEE Trans. Ind. Electron.* **2019**, *66*, 2132–2142. [CrossRef]
24. Pan, Y.; Feng, X.; Zhang, M.; Han, X.; Lu, L.; Ouyang, M. Internal Short Circuit Detection for Lithium-Ion Battery Pack with Parallel-Series Hybrid Connections. *J. Clean. Prod.* **2020**, *255*, 120277. [CrossRef]
25. Feng, X.; He, X.; Lu, L.; Ouyang, M. Analysis on the Fault Features for Internal Short Circuit Detection Using an Electrochemical-Thermal Coupled Model. *J. Electrochem. Soc.* **2018**, *165*, A155–A167. [CrossRef]
26. Feng, X.; Weng, C.; Ouyang, M.; Sun, J. Online Internal Short Circuit Detection for a Large Format Lithium Ion Battery. *Appl. Energy* **2016**, *161*, 168–180. [CrossRef]
27. Barnett, B. Technologies for Detection and Intervention of Internal Short Circuits in Li-Ion Batteries. In Proceedings of the 5th Annual Battery Safety, Washington, DC, USA, 13–14 November 2014.